Characterization and Activity Analysis of Catalytic Water Oxidation Induced by Hybridization of $[(OH_2)(terpy)Mn(\mu\text{-}O)_2Mn(terpy)(OH_2)]^{3+}$ and Clay Compounds

Komei Narita,[†] Takayuki Kuwabara,[†,§] Koji Sone,[†,§] Ken-ichi Shimizu,[‡,||] and Masayuki Yagi*[,†,§]

Faculty of Education and Human Sciences, Niigata University, 8050 Ikarashi-2, Niigata 950-2181, Japan, Graduate School of Science and Technology, Niigata University, 8050 Ikarashi-2, Niigata 950-2181, Japan, and Center for Transdisciplinary Research, Niigata University, 8050 Ikarashi-2, Niigata 950-2181, Japan

Received: June 13, 2006; In Final Form: September 1, 2006

Hybridization of $[(OH_2)(terpy)Mn(\mu\text{-}O)_2Mn(terpy)(OH_2)]^{3+}$ (terpy = 2,2′:6′,2″-terpyridine) (**1**) and mica clay yielded catalytic dioxygen (O_2) evolution from water using a Ce^{IV} oxidant. The reaction was characterized by various spectroscopic measurements and a kinetic analysis of O_2 evolution. X-ray diffraction (XRD) data indicates the interlayer separation of mica changes upon intercalation of **1**. The UV−vis diffuse reflectance (RD) and Mn K-edge X-ray absorption near-edge structure (XANES) data suggest that the oxidation state of the di-μ-oxo Mn_2 core is $Mn^{III}-Mn^{IV}$, but it is not intact. In aqueous solution, the reaction of **1** with a large excess Ce^{IV} oxidant led to decomposition of **1** to form MnO_4^- ion without O_2 evolution, most possibly by its disproportionation. However, MnO_4^- formation is suppressed by adsorption of **1** on clay. The maximum turnover number for O_2 evolution catalyzed by **1** adsorbed on mica and kaolin was 15 and 17, respectively, under the optimum conditions. The catalysis occurs in the interlayer space of mica or on the surface of kaolin, whereas MnO_4^- formation occurs in the liquid phase, involving local adsorption equilibria of adsorbed **1** at the interface between the clay surface and the liquid phase. The analysis of O_2 evolution activity showed that the catalysis requires cooperation of two equivalents of **1** adsorbed on clay. The second-order rate constant based on the concentration (mol g^{-1}) of **1** per unit weight of clay was 2.7 ± 0.1 mol^{-1} s^{-1} g for mica, which is appreciably lower than that for kaolin (23.9 ± 0.4 mol^{-1} s^{-1} g). This difference can be explained by the localized adsorption of **1** on the surface for kaolin. However, the apparent turnover frequency ($(k_{O2})_{app}/s^{-1}$) of **1** on mica was 2.2 times greater than on kaolin when the same fractional loading is compared. The higher cation exchange capacity (CEC) of mica statistically affords a shorter distance between the anionic sites to which **1** is attracted electrostatically, making the cooperative interaction between adsorbed molecules of **1** easier than that on kaolin. The higher CEC is important not only for attaining a higher loading but also for the higher catalytic activity of adsorbed **1**.

Introduction

Natural and synthetic clay compounds are favorable materials for "green" environmental sustainability to which much attention has been paid recently. They consist of hexahedral silicate sheets or octahedral aluminate sheets and cations such as H^+, Li^+, Na^+, K^+, and so forth sandwiched in an interlayer of a nanometer scale between these sheets.[1,2] This unique structural feature is capable of incorporating functional molecules or ions into the interlayer by cation exchange. The interlayer space could be expected as a potential site for a specific chemical reaction that cannot be seen in homogeneous solutions. The expanding and deepening of research related to hybridization of clay compounds with functional molecules could give a guided thought to produce promising novel nanofunctional materials.

Many scientists and engineers have been seeking practical catalysts to activate water for both O_2 and H_2 production, which are indispensable to construction of artificial photosynthetic devices for providing a socially acceptable renewable energy source.[3,4] A development of a catalyst for water oxidation to evolve O_2 (eq 1) is a key task to yield a breakthrough for a technology of water splitting.

$$2H_2O \xrightarrow{\text{water oxidation catalyst}} O_2 + 4H^+ + 4e^- \qquad (1)$$

Water oxidation is catalyzed in photosynthetic oxygen evolving complex (OEC)[5−7] whose active site is known to consist of manganese−oxo cluster. However, the mechanism of water oxidation at OEC is still a question under debate.[5−7] OEC model studies using synthetic manganese complexes are important for providing experimentally proven key reactions for proposals of the water oxidation mechanism by OEC, and the several trailblazing works have been reported to give important key reactions.[3,4,8−15] However, clear demonstrations of the catalytic O_2 evolution from water by synthetic manganese−oxo complexes had not been reported.

Several years ago, Limburg and co-workers reported that O_2 is evolved by the reaction of $[(OH_2)(terpy)Mn(\mu\text{-}O)_2Mn(terpy)(OH_2)]^{3+}$ (terpy = 2,2′:6′,2″-terpyridine) (**1**) with the oxygen donor agent of NaClO or $KHSO_5$.[12,13] Their works have triggered active research fields on syntheses, redox reactions,

* Author to whom correspondence should be addressed. Fax: +81-25-262-7151; e-mail: yagi@ed.niigata-u.ac.jp.
[†] Faculty of Education and Human Sciences.
[‡] Graduate School of Science and Technology.
[§] Center for Transdisciplinary Research.
[||] Present address: Department of Applied Chemistry, Graduate School of Engineering, Nagoya University, Chikusa-ku, Nagoya 464-8603, Japan.

10.1021/jp063679n CCC: $33.50
Published on Web 10/11/2006

catalyses related to **1**, and its derivatives.[16−20] Recently, Baffert et al. reported that electrochemical oxidation of **1** cannot produce O_2 without the oxygen donor agent in solution.[18] We preliminarily reported that the reaction of **1** with a Ce^{IV} oxidant catalytically produces O_2 from water when **1** is adsorbed on kaolin clay.[20] This illustrated a successful design of a heterogeneous catalyst by hybridization of **1** and a clay compound. However, the catalysis by **1** on solid clay matrixes has not yet been sufficiently understood because of only an example for investigation for **1**/kaolin, in which the experimental conditions are unfortunately restricted by a low cation exchange capacity (CEC) of kaolin. Herein, water oxidation catalysis is tested by **1** adsorbed on mica clay which is known to possess an 8∼60 times higher CEC than that of kaolin. This allows not only reliably analyzable spectroscopic data to be gained for characterization of the **1**/clay hybrid but also a wide concentration range to be applied for a kinetic analysis of the catalysis. The catalytic O_2 evolution induced by hybridization of **1** and mica is newly presented and characterized. The kinetic data for **1**/kaolin in a preliminary report[20] is partially included to understand comprehensively the catalysis by **1** on solid clay matrixes. Evidence for catalytic O_2 evolution from water and insights into the unique catalysis, including important influencing factors for the catalytic activity, will be provided.

Experimental Section

Materials. $Mn(NO_3)_2$, $KMnO_4$, $Ce(NH_4)_2(NO_3)_6$ (Wako Pure Chemical Industries, Ltd.), terpy, 2,2′-bipyridine (bpy), and 1,-10-phenanthroline (phen) (Aldrich Chemical Co. Inc.) were purchased and used as received. Kaolin (Aldrich Chemical Co. Inc.) and somasif (ME−100) of mica clay (Co-op Chemical Co., Inc., Japan) were given and used without further purification.

Syntheses of $[(OH_2)(terpy)Mn^{III}(\mu\text{-}O)_2Mn^{IV}(terpy)(OH_2)](NO_3)_3$ (1$(NO_3)_3$), $[(SO_4)(terpy)Mn^{IV}(\mu\text{-}O)_2Mn^{IV}(terpy)(SO_4)]$ (1a), $[(bpy)_2Mn^{III}(\mu\text{-}O)_2Mn^{IV}(bpy)_2](ClO_4)_3$ (2$(ClO_4)_3$), and $[(phen)_2Mn^{III}(\mu\text{-}O)_2Mn^{IV}(phen)_2](ClO_4)_3$ (3$(ClO_4)_3$). **1**$(NO_3)_3$ was prepared by a similar procedure to literature by Collomb et al.[21] An aqueous solution (3 mL, pH = 3.0) of $Mn(NO_3)_2$ (1.7 mmol) was mixed with an aqueous suspension (40 mL, pH = 3.0) of terpy (1.7 mmol) to result in the yellow solution (because of formation of $[Mn(terpy)_2]^{2+}$), and then $KMnO_4$ (0.62 mmol in 5.8 mL water) was dropped into the solution with stirring to give a dark green solution. A saturated $NaNO_3$ (5 mL, pH = 3.0) was added to the solution after filtration. Microcrystalline **1**$(NO_3)_3$ was given by cooling in a refrigerator and was washed with ice water and diethyl ether. (0.44 g, 62% yield) **1a**, **2**$(ClO_4)_3$, and **3**$(ClO_4)_3$ were synthesized according to the literature by Limburg et al.,[13] Cooper and Calvin,[22] and Manchanda et al.,[23] respectively. These complexes were characterized by IR and UV−vis absorption spectra.

Preparations of 1, 2, or 3/Clay Hybrids. To prepare **1**, **2**, or **3**/clay hybrids with the wide-ranging amount of the complexes adsorbed, an aqueous solution (0∼1.2 mM, pH = 4.0) of **1**, **2**, or **3** was added to an aqueous suspension (5∼15 mL, pH = 4.0) of mica or kaolin (50∼400 mg). The resulting suspension was filtrated after stirring for 30 min and then was dried under vacuum to yield a **1**, **2**, or **3**/clay hybrid. The amount of **1**, **2**, or **3** adsorbed was measured by the visible absorption spectral change of the aqueous solution before and after adding clay.

Spectroscopic Measurements. Reactions of **1** with a Ce^{IV} oxidant in an aqueous solution were followed by UV−vis spectral change as measured using a photodiode array spectrophotometer (Shimadzu, Multispec-1500). UV−vis DR spectra of the **1**/mica hybrid were measured using a UV−vis spectrophotometer (JASCO V-550) in a diffuse reflectance mode. XRD patterns of the **1**/clay hybrids were taken in an X-ray diffractometer (MAC Science, MX-Labo). Mn K-edge X-ray absorption near-edge structure (XANES) measurements were carried out in a transmission mode at BL-9A (Photon Factory in High Energy Accelerator Research Organization, Tsukuba, Japan) with a Si(111) double-crystal monochromator. Ionization chambers filled with N_2 for I_0 (17 cm) and N_2 (85%)−Ar (15%) for I (31 cm) were used. High-energy X-rays from high-order reflections were removed by a pair of flat quartz mirrors coated with Rh/Ni that were aligned in parallel. The energy was defined by assigning the first inflection point of the Cu foil spectrum to 8980.3 eV. Normalization of XANES analysis was carried out using REX2000 (Rigaku).

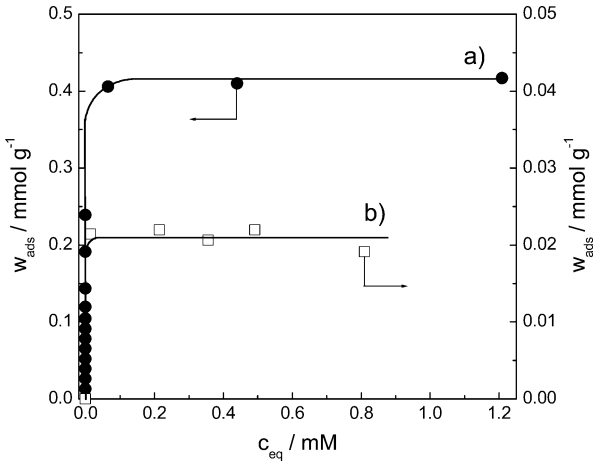

Figure 1. Adsorption isotherms for adsorption of **1** onto (a) mica and (b) kaolin.

O_2 Evolution Experiments. An aqueous solution of **1**, **2**, or **3** was adjusted to pH = 4.0 with HNO_3, and then the adequate small portion of an aqueous solution (1.0 M) of a $Ce(NH_4)_2(NO_3)_6$ oxidant was added to the solution. Otherwise, to the aqueous suspension containing 10∼75 mg of the **1**, **2**, or **3**/clay hybrid was added the adequate small portion of the aqueous solution of Ce^{IV}. The reaction was typically followed in 2.0 mL of a liquid-phase volume at pH = 1.0 and 25 °C under the conditions of a large excess (50∼100 mM) of Ce^{IV} versus **1** (pH of the **1** solution changes to 1.0 by adding a Ce^{IV}). The amount of O_2 evolved was analyzed using a Clark type oxygen electrode (Hansatech Instruments, Oxygraph OXYG1 and DW1/AD unit) with 1 μM of the detection level of O_2 dissolved in water. Gas chromatograph (Shimadzu, GC-8A) equipped with a 5 Å molecular sieve column (argon carrier gas) was used to analyze more than the O_2 amount restricted for our oxygen electrode instrument because of release of O_2 gas from the electrode. For ^{18}O-labeling experiments using $H_2{}^{18}O$, the evolved gas was analyzed on an electron-impact-ionization mass spectrometer (JEOL, JMS-SX102).

Results and Discussion

Adsorption of 1 onto Clay Compounds. When an aqueous solution of **1** was added to an aqueous suspension of mica or kaolin, **1** was adsorbed onto clay by cation exchange with Na^+. The adsorption isotherms of **1** onto mica and kaolin are shown in Figure 1. The concentration (w_{ads}/mol g^{-1}) of **1** adsorbed on clay rose steeply at very low (almost zero) equilibrium concentration (c_{eq}/M) of **1** in the solution, indicating the high

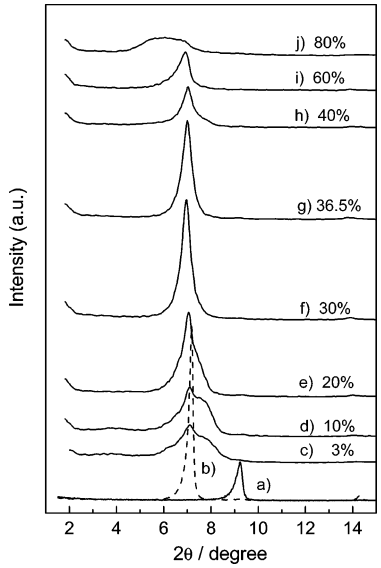

Figure 2. XRD patterns of mica and **1**/mica hybrids. (a) Dry mica and (b) mica kept in aerobic conditions. The **1** concentration, w_{ads} (f_{ads}), for **1**/mica hybrids are (c) 0.012 (3%), (d) 0.041 (10%), (e) 0.082 (20%), (f) 0.12 (30%), (g) 0.15 (36.5%), (h) 0.16 (40%), (i) 0.25 (60%), and (j) 0.33 mmol g^{-1} (80%).

adsorption equilibrium constant of **1** onto clays. The maximum concentration ($(w_{ads})_{max} = 0.411$ mmol g^{-1}) of **1** adsorbed onto mica was 20 times higher than that (0.022 mmol g^{-1}) for kaolin. These values are consistent with CEC of mica (1.2 meq g^{-1}) and kaolin (0.02∼0.15 meq g^{-1}) when considering trivalence of **1** cation. The fractional loading (f_{ads}%) of **1** onto clay was defined as $f_{ads}\% = w_{ads}/(w_{ads})_{max}$ and was used in some cases for convenience.

Characterization of a 1/Mica Hybrid. *XRD Spectroscopic Measurements.* An XRD spectroscopic technique was used to evaluate the layer structure of mica and kaolin adsorbing **1**. The XRD pattern of kaolin with an intense sharp peak at $2\theta = 12.36$ degrees did not change by adsorption of **1**, showing that **1** does not change the layer structure of kaolin. **1** is considered to be adsorbed onto the surface of kaolin. By contrast, the XRD pattern of mica changed drastically by adsorption of **1**, as shown in Figure 2. The XRD pattern (Figure 2a) of dry mica gave an intense peak at $2\theta = 9.2$ degrees, corresponding to an interlayer distance of 9.56 Å. However, when mica was kept in air, the peak shifted to $2\theta = 7.18$ degrees (interlayer distance of 12.3 Å) by hydration of Na^+ ions (Figure 2b). The XRD pattern of the **1**/mica hybrid exhibited a peak at $2\theta = 7.12$ degrees and a shoulder at $2\theta = 7.92$ degrees in the low concentration ($w_{ads} = 0.012$ mmol g^{-1}, $f_{ads} = 3\%$) of adsorbed **1**. As the concentration increased, the peak intensity increased, indicating that **1** is intercalated into the interlayer of mica. At $w_{ads} = 0.12$ mmol g^{-1} ($f_{ads} = 30\%$), the shoulder almost disappeared, resulting in an intense and sharp peak at $2\theta = 6.96$ degrees (interlayer distance of 12.7 Å). The peak was lowered at $f_{ads} = 60\%$ and ultimately became very broad at $2\theta = 6.9$∼5.4 degrees at $f_{ads} = 80\%$. The more ordered layer structure was given at $f_{ads} = 30\%$ relative to the other concentrations (except $f_{ads} = 0\%$). The interspace distance between the layers at $f_{ads} = 30\%$ can be given as 6.1 Å from the interlayer distance (12.7 Å) and the thickness (6.6 Å) of the layer. This is consistent with the molecular size of **1** (13.2 × 11.1 × 4.8 Å) on the basis of crystal graphic data and van der Waals radius (1.2 Å) of a hydrogen atom.

UV−Vis DR Spectroscopic Measurements. The UV−vis DR spectrum of the **1**/mica hybrid exhibited a peak at 406 nm. This

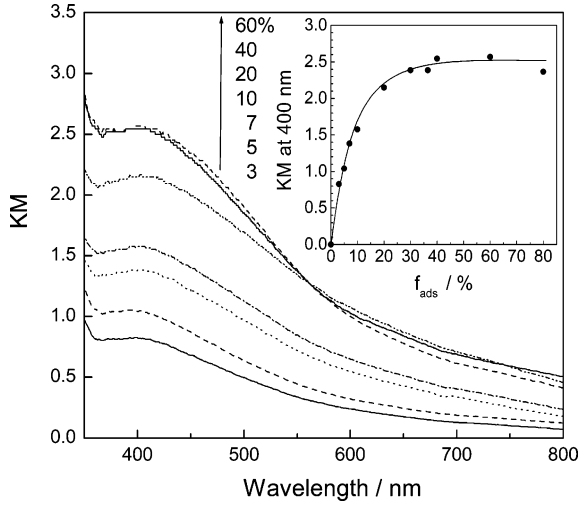

Figure 3. UV-vis DR spectra of **1**/mica hybrids with various w_{ads} (f_{ads}) as indicated on figure. Inset shows the plots of Kubelka−Munk at 400 nm vs f_{ads}.

is different from the DR spectrum of **1** (as a powder) with a shoulder at 414 nm and peaks at 556 and 662 nm, suggesting that adsorbed **1** is not intact on mica. Figure 3 shows the UV−vis DR spectra of the **1**/mica hybrid with the various concentrations of **1** adsorbed. The Kubelka−Munk (KM) values increased almost linearly with f_{ads} below $f_{ads} = 20\%$ (inset of Figure 3), with the unchanged peak wavelength ($\lambda_{max} = 406$ nm) and spectral shape in the whole concentrations employed. This indicates that the different spectrum between **1** and **1**/mica hybrid is independent of its concentration on mica. The KM values plateaued at more than $f_{ads} = 20\%$. This can be explained by a sort of a filter effect; the species close to the mica surface could absorb light sufficiently under the high f_{ads} conditions, so that light absorption of the deeply intercalated species could not be reflected in the KM values.

The Mn K-Edge XANES Measurements. The Mn K-edge XANES spectra of the **1**/mica hybrid are shown in Figure 4, including those of **1** ($Mn^{III}−Mn^{IV}$) and $[(SO_4)(terpy)Mn^{IV}(\mu\text{-}O)_2Mn^{IV}(terpy)(SO_4)]$ **(1a)** ($Mn^{IV}−Mn^{IV}$) as powders. The XANES spectrum of the **1**/mica hybrid ($w_{ads} = 0.082$ mmol g^{-1}, $f_{ads} = 20\%$) exhibited a shoulder at 6551.1 eV and a peak at 6561.6 eV, which are almost identical to that for $f_{ads} = 60\%$ (a shoulder at 6550.9 eV and a peak at 6561.6 eV). This is consistent with the UV−vis DR spectroscopic data independent of the concentration of **1** (vide supra). It is well-known that the Mn K-edge shifts to a high-energy region by an increase in an oxidation state of Mn centers in a di-μ-oxo Mn_2 complex.[24] The comparison in the Mn K-edge among the **1**/mica hybrid, **1**, and **1a** could provide an insight into the oxidation state of Mn centers in the adsorbed species on mica. K-edge energy was evaluated by energy at the local minimum around 6551 eV for the second-order derivative Mn K-edge XANES spectra (a lower item in Figure 4). The Mn K-edge energy (6551.1 eV) of **1** was lower by 2.0 eV than that (6553.1 eV) of **1a**. This is consistent with the result reported by Visser et al. on Mn K-edge XANES measurements of $[(phen)Mn(\mu\text{-}O)_2Mn(phen)]^{3+/4+}$ in an acetonitrile solution, in which the K-edge shifted to a high-energy region by 2.2 eV in oxidation from the $Mn^{III}−Mn^{IV}$ to $Mn^{IV}−Mn^{IV}$ states of the di-μ-oxo Mn_2 core.[24] The K-edges (6551.1 eV for $f_{ads} = 20\%$, 6550.9 eV for $f_{ads} = 60\%$) for the **1**/mica hybrid were almost identical to that (6551.1 eV) of **1** rather than that of **1a**. This suggests that the oxidation state of the di-μ-oxo Mn_2 core in the adsorbed species on mica could be $Mn^{III}−Mn^{IV}$.[25]

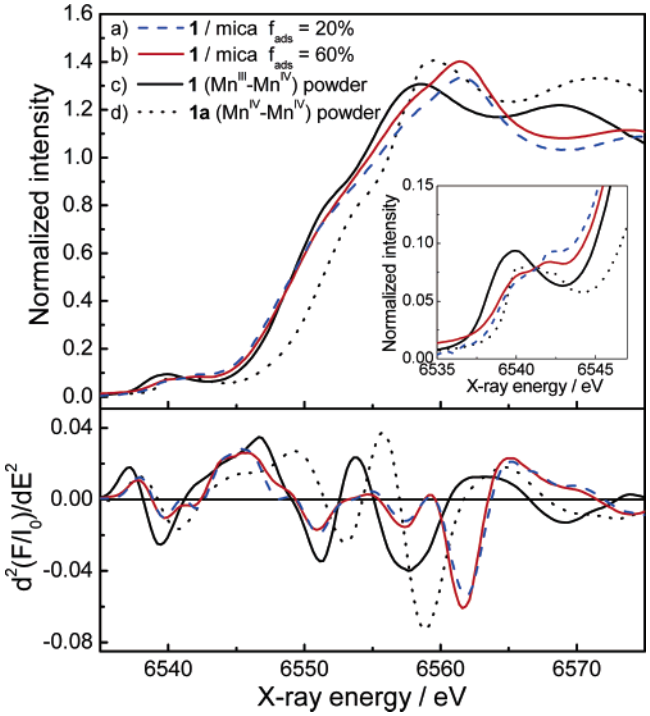

Figure 4. Mn K-edge XANES spectra (upper) and the second-order derivative spectra (lower). (a) **1**/mica with $w_{ads} = 0.082$ mmol g^{-1} ($f_{ads} = 20\%$), (b) **1**/mica with $w_{ads} = 0.25$ mmol g^{-1} ($f_{ads} = 60\%$), (c) **1** powder, and (d) **1a** powder. The inset is the magnified spectra for the pre-edge peak around 6540 eV.

The magnified spectra in the range of 6535∼6547 eV are shown in the inset of Figure 4 for the pre-edge peak around 6540 eV, assigned to a dipole-forbidden 1s → 3d transition of the Mn center. The spectrum of **1** exhibited a pre-edge peak at 6539.3 eV, while the spectra of the **1**/mica hybrid exhibit two separate pre-edge peaks at 6539.8 and 6542.1 eV. Pre-edge peak energy corresponds to the energy difference between the 1s level and the unoccupied 3d levels of the center ion, the latter of which are influenced by the ligand field.[26−28] The higher pre-edge energy (at 6542.1 eV) for the **1**/mica hybrid could be explained by an increase of the unoccupied 3d levels, possibly because of a distorted local coordination structure of Mn ions. However, it is also established that pre-edge peak energy depends on the valence state of the center ions; pre-edge peak energy shifts to higher energy with an increase in the oxidation number of iron.[29−31] The possible explanation by the higher valence state could not be excluded for the higher pre-edge energy in Mn K-edge XANES spectra of the **1**/mica hybrid. We are considering a significant distortion of **1** adsorbed on mica. However, it is still unproven whether it can rationalistically explain the UV−vis DR spectroscopic features (Figure 3).

Reactions of 1 with a Ce^{IV} Oxidant in Water. Reactions of **1** with a Ce^{IV} oxidant in water were investigated using a UV−vis absorption spectroscopic technique. The absorption spectral change in a reaction of **1** with 1 equiv of Ce^{IV} shows the absorption increase at 440 nm and the absorption decrease at 700 nm with an isosbestic point of 580 nm. This is close to the absorption spectral change in formation of $[(OH_2)(terpy)Mn^{IV}(\mu\text{-}O)_2Mn^{IV}(terpy)(OH_2)]^{4+}$ ($Mn^{IV}-Mn^{IV}$) by disproportionation of **1** promoted by a pH decrease, as reported by Chen et al.[17] (The absorbance at 450 nm increased and the absorption at 660 nm decreased with an isosbestic point at 565 nm.) This result suggests that the reaction of **1** with 1 equiv of Ce^{IV} stoichiometrically produces $Mn^{IV}-Mn^{IV}$ in solution.[32] The

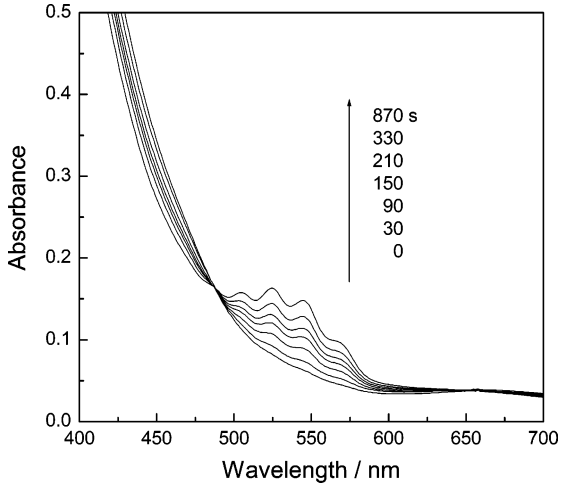

Figure 5. Visible absorption spectral change of an aqueous solution containing 0.1 mM **1** and 2.0 mM Ce^{IV} ion at pH = 1.0 and 25 °C. Reaction time was indicated on figure.

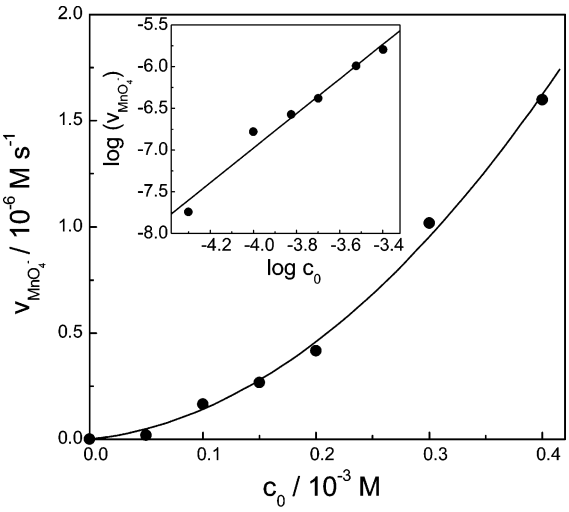

Figure 6. Plots of initial rate (v_{MnO4-}) of MnO_4^- formation vs concentration (c_0) of **1**. Inset shows plots of log v_{MnO4-} vs log c_0. Concentration of Ce^{IV}, 10 mM; pH = 1.0; 25 °C.

spectral change in a reaction with 8 equiv of Ce^{IV} exhibited the appearance of the absorption band at $\lambda_{max} = 545$ nm with vibration structures that are a characteristic feature of MnO_4^- ion, concomitantly with the formation of the $Mn^{IV}-Mn^{IV}$ species. In a reaction with 20 equiv of Ce^{IV}, stoichiometric formation of MnO_4^- from **1** was indicated by appearance of the absorption band at $\lambda_{max} = 545$ nm with an isosbestic point at 489 nm, as shown in Figure 5.

To reveal the mechanism of MnO_4^- formation, its kinetics was studied under the conditions of a large excess of Ce^{IV}. The initial rate (v_{MnO4-}) of MnO_4^- formation was given from the initial slope of the absorbance change at $\lambda_{max} = 545$ nm ($\epsilon = 2344$ M^{-1} cm^{-1}). It increased with the concentration (c_0) of **1** as shown in Figure 6, and the plots of log v_{MnO4-} versus log c_0 gave a straight line with the slope of 2.07 ± 0.17 and intercept $= 1.32 \pm 0.66$ (inset of Figure 6). The slope shows that MnO_4^- formation can be analyzed as a second-order reaction with respect to **1**. It is most possibly formed by disproportionation of the high oxidation state of **1** in a rate-determining step. The second-order rate constant for MnO_4^- formation was calculated to be 2.1×10^1 M^{-1} s^{-1} from the intercept.

O_2 evolution by **1** from water was tested in an aqueous solution containing 0.1∼0.5 mM **1** and a large excess (100 mM)

TABLE 1: Summary of Amount (n_{O2}) of O_2 Evolved and Turnover Number (TN) of Complexes for O_2 Evolution Experiments[a]

compounds	n_{ads}/μmol	clay	amount of clay/mg	n_{O2}/μmol	TN
$[Mn_2(\mu\text{-}O)_2(terpy)_2(OH_2)_2]^{3+}$ (**1**)	1.0	no[b]		0.0	0.0
	5.0	no[b]		0.0	0.0
	50.0	no[b]		0.0	0.0
	0.0	kaolin	50	0.0	
	0.13	kaolin	50	2.2 (±0.21)	17 (±1.6)
	0.26	kaolin	50	3.4 (±0.02)	13 (±0.1)
	0.46	kaolin	50	6.6 (±0.53)	14 (±1.2)
	0.0	mica	10	0.0	
	0.25	mica	10	0.95	3.8
	0.50	mica	10	3.7 (±0.15)	7.3 (±0.3)
	1.0	mica	10	15 (±0.6)	15 (±0.6)
	1.5	mica	10	23 (±1.5)	15 (±1.0)
$[Mn_2(\mu\text{-}O)_2(bpy)_4]^{3+}$ (**2**)	1.0	no[b]		0.0	0.0
	0.46	kaolin	50	0.26 (±0.01)	0.52 (±0.02)
	1.5	mica	10	1.0 (±0.02)	0.68 (±0.01)
$[Mn_2(\mu\text{-}O)_2(phen)_4]^{3+}$ (**3**)	1.0	no[b]		0.0	0.0
	0.46	kaolin	50	0.26 (±0.01)	0.57 (±0.02)
	1.5	mica	10	0.71 (±0.12)	0.47 (±0.08)
MnO_4^-	10.0	no[b]		0.0	0.0
MnO_2	10.0	no[c]		0.0	0.0
Mn^{2+}	0.92	no[b]		0.0	0.0
	0.92	kaolin	50	0.0	0.0
$terpyH_n^{n+}$	0.92	kaolin	50	0.0	0.0

[a] Reaction conditions are as follows: the amount of Ce^{IV} oxidant, 1.0 mmol; reaction time, 4 days; liquid-phase volume, 10 mL; gas-phase volume, 3 mL. n_{O2} was measured using a gas chromatograph. [b] Homogeneous solution. [c] Suspension.

of Ce^{IV} oxidant, but it was not observed at all, nor was O_2 evolved using a 10∼50-fold larger concentration of **1** (5 mM **1**, 100 mM Ce^{IV}) (see Table 1).

Reactions of 1/Clay Hybrids with a Ce^{IV} Oxidant in Water. Reactions of the **1**/clay hybrids with a large excess Ce^{IV} oxidant in water produced a significant amount of O_2 in contrast to no O_2 evolution by **1** in solution. Data on O_2 evolution are summarized in Table 1. O_2 evolution was not observed when using mica without **1** as a control. The amount (n_{O2}/mol) of O_2 evolved increased with the amount (n_{ads}/mol) of **1** adsorbed on either kaolin or mica, showing that O_2 is evolved by **1** adsorbed on clay. The maximum turnover number (TN) of **1** was almost the same for mica (TN = 15) and kaolin (TN = 17). This result corroborates that **1** adsorbed on clay catalyzes O_2 evolution. To define the catalysis, similar O_2 evolution experiments were extended to various manganese species including MnO_2, Mn^{2+}, and MnO_4^- in water, as well as adsorbed $Mn^{2+}$and $terpyH_n^{n+}$ on mica or kaolin. In none of the trials using these species was O_2 evolution detected. These results show the unique catalysis by **1** adsorbed on the clay.

$[(bpy)_2Mn^{III}(\mu\text{-}O)_2Mn^{IV}(bpy)_2]^{3+}$ (**2**) and $[(phen)_2Mn^{III}(\mu\text{-}O)_2\text{-}Mn^{IV}(phen)_2]^{3+}$ (**3**) have comparable structures with **1** but no terminal water ligands. The similar experiments were carried out using **2** or **3** in solution and on clays to compare with the reactions of **1** with a Ce^{IV} oxidant. For neither **2** nor **3** was O_2 evolved in the solution, but it was for both **2**/clay and **3**/clay. However, TN values are less than unity for **2**/clay (TN = 0.5∼0.7) and for **3**/clay (TN = 0.5∼0.6),[33] showing that neither **2** nor **3** adsorbed on clay works as a catalyst for O_2 evolution. This result suggests that terminal water coordination sites could be important for the catalysis by adsorbed **1**.

For clay hybrid systems, the MnO_4^- ion formed by decomposition of **1** was also observed in a liquid phase after removal of the clay hybrids by centrifugation.[34] The amount (n_{MnO4-}/mol) and yield (Φ_{MnO4-}) of MnO_4^- formed for a 30-min reaction are summarized in Table 2 including the data for the solution. Φ_{MnO4-} was 56.3∼85.8% in solutions under the conditions. However, Φ_{MnO4-} (18.3∼31.3%) for the **1**/clay hybrids was much less than in solutions under the comparable conditions. This shows that adsorption of **1** onto the clay significantly suppresses the decomposition of **1** to form MnO_4^-.

TABLE 2: Summary of Amount (n_{MnO4-}) and Yield (Φ_{MnO4-}) of MnO_4^- Formed in Reactions of 1 and a Ce^{IV} Oxidant[a]

system	amount of clay/mg	$n_{ads}/10^{-7}$ mol	n_{MnO4-}[b]$/10^{-7}$ mol	Φ_{MnO4-}[c] %
homogeneous solution		1.2	0.90	75.0
		2.4	2.1	85.8
		4.8	2.7	56.3
1/kaolin	75	1.5	0.47	31.3
	75	3.0	0.77	25.7
	75	7.0	1.3	18.3
1/mica	10	4.8	0.95	19.8
	40	4.8	1.2	24.6
	75	5.1	0.97	19.0

[a] Reaction conditions are as follows: the concentration of Ce^{IV} oxidant, 50 mM; reaction time, 30 min; liquid-phase volume, 2 mL. [b] n_{MnO4-} was measured from absorbance at λ_{max} = 545 nm (ϵ = 2344 M^{-1} cm^{-1}). [c] Φ_{MnO4-} was defined as n_{MnO4-} normalized by n_{ads}.

^{18}O-Labeling O_2 Evolution Experiments using $H_2{}^{18}O$. To identify an oxygen atom source for O_2 evolution, ^{18}O-labeling experiments were carried out using $H_2{}^{18}O$, and the evolved gas was analyzed on an electron-impact-ionization mass (EIM) spectrometer. In a $H_2{}^{18}O$ media (47.5 and 23.8 v/v % $H_2{}^{18}O$), the EIM spectra gave the peaks at m/z = 34 and 36, corresponding to $^{16}O^{18}O$ and $^{18}O_2$, additionally to the peak for $^{16}O_2$ at m/z = 32, in contrast to no peaks at m/z = 34 and 36 for natural abundance water. (Figure 7) The amounts of $^{16}O_2$, $^{16}O^{18}O$, and $^{18}O_2$ are analyzed from the intensities at m/z = 32, 34, and 36, respectively. The O_2 evolution data are summarized in Table 3. The content fraction (Φ_{18O}) of an ^{18}O atom in O_2 evolved is consistent with the ^{18}O content in the water media. It was thus corroborated that the oxygen atoms in O_2 evolved are exclusively originated from water.

Kinetic Analysis and Influencing Factors of the O_2 Evolution for the 1/Clay Hybrids. The time course of O_2 evolved in the reaction of **1**/mica with a large excess Ce^{IV} ion is shown in Figure 8, including data for a homogeneous solution

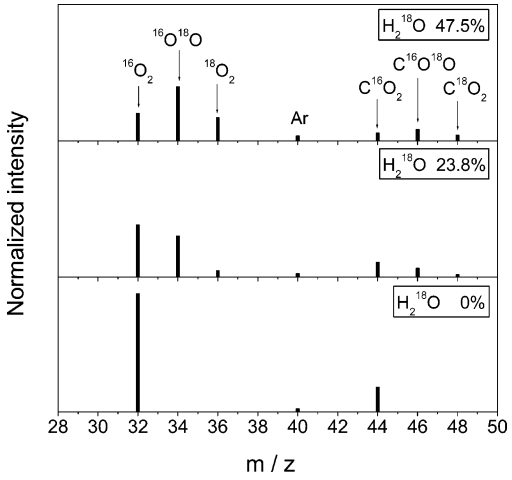

Figure 7. Electron-impact-ionization mass (EIM) spectra for ^{18}O-labeling O_2 evolution experiments using **1**/kaolin (75 mg) with w_{ads} = 9.3 μmol g^{-1}; reaction time, 7 days; liquid volume, 1.0 mL; gas-phase volume, 6.3 mL.

TABLE 3: Summary of O_2 Evolution Data in ^{18}O-Labeling Experiments Using 1/Kaolin[a]

	n_{O2}/μmol[b]			
$H_2{}^{18}O$ v/v %	$^{16}O_2$	$^{16}O^{18}O$	$^{18}O_2$	Φ_{18O}[c] %
0	5.6	0	0	0
23.8	2.7	1.6	0.24	23
47.5	1.9	2.4	1.0	41

[a] Kaolin, 75 mg; n_{ads} = 0.7 μmol; reaction time, 7 days; liquid volume, 1.0 mL; gas-phase volume, 6.3 mL. [b] Obtained from intensity at m/z = 32, 34, and 36 using calibration on O_2 abundance. [c] Φ_{18O} is fraction of ^{18}O atom in O_2 evolution.

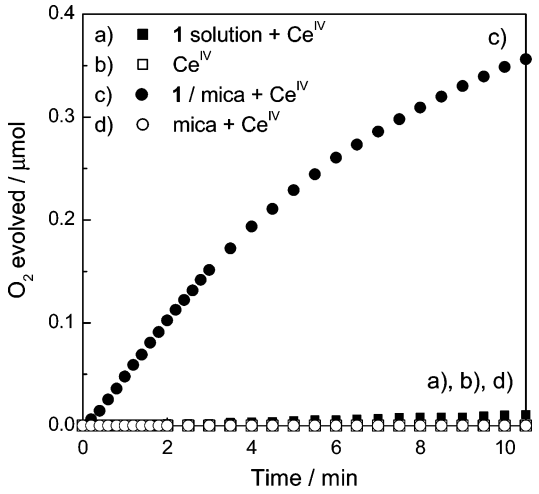

Figure 8. Time courses of the amount of O_2 evolved in reactions of **1** and a 50 mM Ce^{IV} oxidant. (a) Aqueous solution of **1** (1.5 μmol; 0.75 mM), (b) aqueous solution without **1**, (c) aqueous suspension of mica clay (10 mg) adsorbing 1.5 μmol **1** (w_{ads} = 0.15 mmol g^{-1}; f_{ads} = 36.5%), and (d) aqueous suspension of mica clay (10 mg) without **1**. Liquid volume, 2.0 mL; pH = 1.0.

of **1** containing the same amount (1.5 μmol) of **1** for comparison. The initial O_2 evolution rate (v_{O2}/mol s^{-1}) was calculated from the initial slope of the time course. The inset in Figure 9 shows the comparison of v_{O2} between the **1**/mica and the **1**/kaolin hybrids (both clay amounts are 75 mg). The n_{ads} range for **1**/mica is much wider than that for **1**/kaolin, and the maximum v_{O2} value for the former is 7.6 times higher than that for the latter under the conditions employed (n_{ads} < 8 μmol). This result is ascribed to the higher CEC of mica.

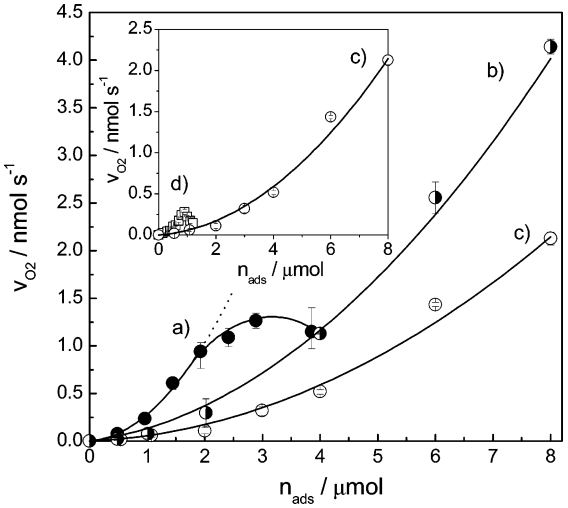

Figure 9. Plots of initial rate (v_{O2}/mol s^{-1}) of O_2 evolution vs the amount (n_{ads}) of **1** for the various amounts of mica. The amounts of mica are (a) 10 mg (closed circles), (b) 40 mg (half-closed circles), and (c) 75 mg (open circles) for **1**/mica. 50 mM Ce^{IV}; liquid volume, 2.0 mL; pH = 1.0. The inset shows the magnified figure for comparison between **1**/mica and **1**/kaolin. Open circles in the inset are the same data as plots (c) for **1**/mica (75 mg). Open squares are (d) v_{O2} data for **1**/kaolin (75 mg). The same v_{O2} data in a low n_{ads} region for **1**/kaolin (open squres) were cited from ref 20.

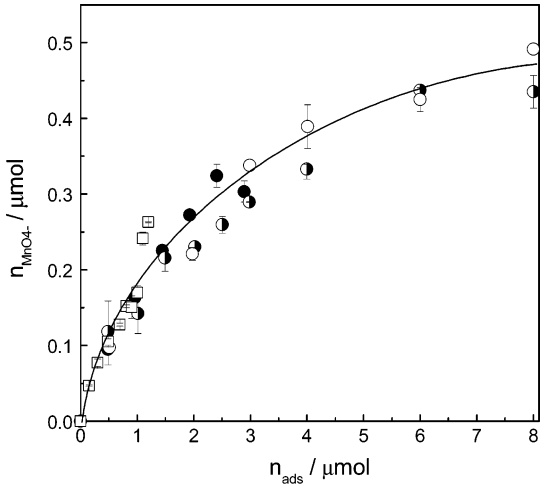

Figure 10. Plots of amount (n_{MnO4-}) of MnO_4^- formed vs the amount (n_{ads}) of **1** for various amounts of clay. The amounts of mica are (a) 10 mg (closed circles), (b) 40 mg (half-closed circles), and (c) 75 mg (open circles) for **1**/mica. (d) 75 mg (open squares) for **1**/kaolin, 50 mM Ce^{IV}; liquid volume, 2.0 mL; pH = 1.0. n_{MnO4-} was measured after a 30-min reaction.

The plots of v_{O2} versus n_{ads} are shown in Figure 9 for **1**/mica with various amounts of mica (10∼75 mg). v_{O2} increased upward with n_{ads} under the conditions employed for 40 and 75 mg mica. However, v_{O2} for 10 mg mica thereafter departed from the upward curvature above n_{ads} = 2.0 μmol, which is ascribed to elution of **1** from mica into a liquid phase to promote decomposition of **1** to MnO_4^- ion. v_{O2} was higher as the amount of mica is lower comparing the same n_{ads} below n_{ads} = 2.0 μmol. (v_{O2} order: 10 > 40 > 75 mg).

On the other hand, n_{MnO4-} measured in parallel with the v_{O2} increased with n_{ads}, as shown in Figure 10.[35] In contrast to the v_{O2} data (Figure 9), the profiles of n_{MnO4-} versus n_{ads} were the same between **1**/kaolin and **1**/mica and were independent of the amount of mica. These results suggest that MnO_4^- formation from adsorbed **1** takes place in the liquid phase, whereas the catalytic O_2 evolution takes place in the interlayer space of the

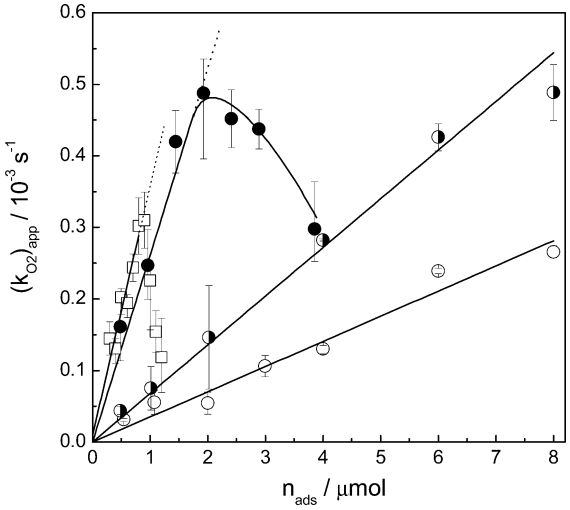

Figure 11. Plots of $(k_{O2})_{app}$ vs the amount (n_{ads}) of **1**. The amounts of mica are (a) 10 mg (closed circles), (b) 40 mg (half-closed circles), and (c) 75 mg (open circles) for **1**/mica and (d) 75 mg (open squares) for **1**/kaolin. The conditions are indicated in Figure 9.

mica. There could be local adsorption equilibria of adsorbed **1** at the interface between the clay surface and the liquid phase. MnO_4^- prefers to be formed in the liquid phase rather than on the clay. This is supported by MnO_4^- formation suppressed by the adsorption of **1** on the mica. (vide supra) MnO_4^- formation might still occur on clay, but it could be much slower relative to the O_2 evolution.

The upward curvature in v_{O2} versus n_{ads} plots (Figure 9) shows that the specific O_2 evolution increases with increasing n_{ads}. The O_2 evolution was analyzed by the kinetic model (eq 2) assuming on combination between first- and second-order O_2 evolutions with respect to the adsorbed **1**:

$$v_{O2} = k_1 n_{ads} + k_2 n_{ads}^2 \quad (2)$$

where k_1/s^{-1} and k_2/mol^{-1} s^{-1} are first-order and second-order rate constants for O_2 evolution, respectively. For comparison of the turnover frequency of **1** adsorbed on clays, v_{O2} was normalized by n_{ads} to define the apparent turnover frequency, $(k_{O2})_{app}$/s^{-1}, as eq 3.

$$(k_{O2})_{app} = v_{O2}/n_{ads} = k_1 + k_2 n_{ads} \quad (3)$$

The plots of $(k_{O2})_{app}$ versus n_{ads} gave the straight lines with significant slopes passing through the origin for each **1**/clay (at $n_{ads} < 2.0$ μmol for 10 mg mica and at $n_{ads} < 0.9$ μmol for **1**/kaolin), as shown in Figure 11. The significant slope (corresponding k_2 in eq 3) suggests that O_2 is predominantly evolved by a bimolecular reaction of **1** adsorbed on clay. It is most likely that adsorbed **1** works cooperatively for the catalysis. It may take place by intermolecular coupling of Mn^V=O that could be formed by successive oxidation of a terminal water ligand on **1**, on the basis of noncatalytic activity of **2** and **3** for O_2 evolution. However, no evidence for involvement of Mn^V=O in the catalysis is obtained. The fitting of eq 3 to the $(k_{O2})_{app}$ data yielded almost zero for the k_1 and the k_2 values depending on the amount of mica ($(2.7 \pm 0.3) \times 10^2$, $(0.69 \pm 0.01) \times 10^2$, and $(0.34 \pm 0.03) \times 10^2$ mol^{-1} s^{-1} for 10, 40, and 75 mg mica, respectively).

All the $(k_{O2})_{app}$ data for 10∼40 mg mica were replotted versus concentration w_{ads} (mol g^{-1}) instead of n_{ads} (mol) in Figure 12. The plots exhibited the significant linearity below 0.2 mmol g^{-1}, showing that $(k_{O2})_{app}$ is principally related to w_{ads}. The slope

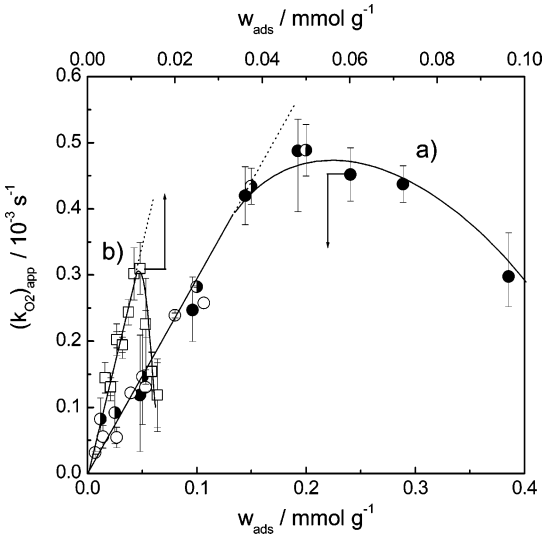

Figure 12. Plots of $(k_{O2})_{app}$ vs the concentration (w_{ads}) of **1**. (a) **1**/mica; 10 mg (closed circles), 40 mg (half-closed circles), and 75 mg (open circles). (b) **1**/kaolin; 75 mg (open squares).

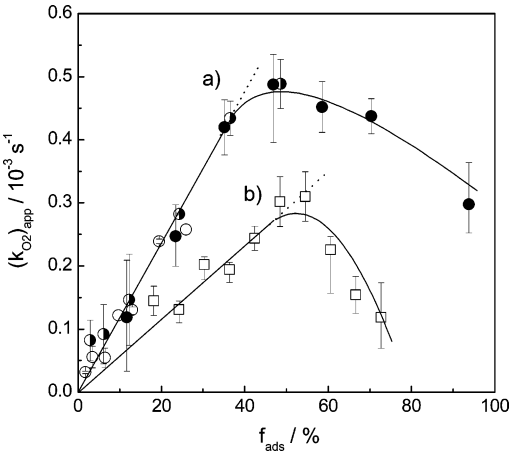

Figure 13. Plots of $(k_{O2})_{app}$ vs the loading amount (f_{ads}) of **1**. (a) **1**/mica; 10 mg (closed circles), 40 mg (half-closed circles, and 75 mg (open circles). (b) **1**/kaolin; 75 mg (open squares).

of the linear plots of $(k_{O2})_{app}$ versus w_{ads} yields $k_2' = 2.7 \pm 0.1$ mol^{-1} s^{-1} g of a second-order rate constant on the basis of w_{ads}. For comparison, $(k_{O2})_{app}$ for **1**/kaolin was plotted versus w_{ads} in Figure 12 together. The k_2' for **1**/kaolin was 23.9 ± 0.4 mol^{-1} s^{-1} g, which is 8.9 times higher than that for **1**/mica. This difference could be explained by localized adsorption of **1** on the kaolin surface. For **1**/mica, **1** is intercalated into an interlayer as well as adsorbed on a surface of mica (see Figure 2). On the other hand, **1** is adsorbed only on a surface for **1**/kaolin (vide supra), resulting in a localized adsorption of **1** on the kaolin surface. Nevertheless, the maximum $(k_{O2})_{app}$ for **1**/mica was higher than that for **1**/kaolin under respective optimum conditions. This is attributed to the higher loading of **1** because of the higher CEC of mica.

To reveal the influence of CEC on $(k_{O2})_{app}$, it was replotted versus f_{ads}% in Figure 13 for both the **1**/mica and the **1**/kaolin hybrids. The $(k_{O2})_{app}$ increased linearly at a low f_{ads} region, and the maximum $(k_{O2})_{app}$ was observed around $f_{ads} = 50\%$ for both the hybrids. The $(k_{O2})_{app}$ for **1**/mica was 2.2 times higher in average (in the slope of the line) than that for **1**/kaolin comparing the same f_{ads}. This can be explained by considering the statistical distance between anionic sites on clay to which **1** is attracted electrostatically. The higher CEC of mica statistically affords a shorter distance between the anionic sites, making the coopera-

tive interaction between adsorbed molecules of **1** easier than that on kaolin. The higher CEC is important not only for attaining a higher loading but also for the higher catalytic activity of adsorbed **1**.

Conclusion

The present paper illustrates evidence of catalytic O_2 evolution from water induced by adsorption of **1** onto solid clay. It requires cooperative interaction of two equivalents of **1** adsorbed. The catalysis occurs in the interlayer space of mica or on the surface of kaolin, whereas the decomposition of **1** to form MnO_4^- ions occurs in the liquid phase, involving local adsorption equilibria of adsorbed **1** at the interface between the clay surface and the liquid phase. Nevertheless, MnO_4^- formation is suppressed by adsorption of **1** on clay. The concentration and localization of **1** adsorbed on clay, as well as the distance between anionic sites on clay statistically related to its cation exchange capacity, are the important factors for the cooperative catalysis. These results undoubtedly provide a first step for development of nanohybrid catalysts for water oxidation to evolve O_2 using clay compounds.

Acknowledgment. Research was supported by Grant-in-Aid for Young Scientists (B) from the Ministry of Education, Culture, Sports, Science, and Technology (No. 16750113) and grant from the Nissan Science Foundation. We thank Dr. T. Sato for help with EIMS spectroscopic measurements. The X-ray absorption experiments were performed under the approval of the Photon Factory Program Advisory Committee (Proposal No. 2005G-189).

References and Notes

(1) *Clay Surfaces - Fundamentals and Applications*; Wypych, F., Satyanarayana, K. G., Eds.; Academic Press Inc: San Diego, CA, 2004.

(2) Ogawa, M.; Kuroda, K. *Chem. Rev.* **1995**, *95*, 399.

(3) Ruettinger, W.; Dismukes, G. C. *Chem. Rev.* **1997**, *97*, 1.

(4) Yagi, M.; Kaneko, M. *Chem. Rev.* **2001**, *101*, 21.

(5) Ferreira, K. N.; Iverson, T. M.; Maghlaoui, K.; Barber, J.; Iwata, S. *Science* **2004**, *303*, 1831.

(6) Photosynthetic Water Oxidation special issue. In *Biochim. Biophys. Acta-Bioenerg.*; Nugent, J., Ed.; 2001; Vol. 1503.

(7) Loll, B.; Kern, J.; Saenger, W.; Zouni, A.; Biesiadka, J. *Nature (London)* **2005**, *438*, 1040.

(8) Ramaraj, R.; Kira, A.; Kaneko, M. *Angew. Chem., Int. Ed. Engl.* **1986**, *25*, 825.

(9) Ramaraj, R.; Kira, A.; Kaneko, M. *Chem. Lett.* **1987**, 261.

(10) Ruettinger, W.; Yagi, M.; K. Wolf; Bernasek, S.; Dismukes, G. C. *J. Am. Chem. Soc.* **2000**, *122*, 10353.

(11) Yagi, M.; Wolf, K. V.; Baesjou, P. J.; Bernasek, S. L.; Dismukes, G. C. *Angew. Chem., Int. Ed.* **2001**, *40*, 2925.

(12) Limburg, J.; Vrettos, J. S.; Liable-Sands, L. M.; Rheingold, A. L.; Crabtree, R. H.; Brudvig, G. W. *Science* **1999**, *283*, 1524.

(13) Limburg, J.; Vrettos, J. S.; Chen, H. Y.; de Paula, J. C.; Crabtree, R. H.; Brudvig, G. W. *J. Am. Chem. Soc.* **2001**, *123*, 423.

(14) Naruta, Y.; Sasayama, M.; Sasaki, T. *Angew. Chem., Int. Ed. Engl.* **1994**, *33*, 1839.

(15) Shimazaki, Y.; Nagano, T.; Takesue, H.; Ye, B.-H.; Tani, F.; Naruta, Y. *Angew. Chem., Int. Ed.* **2004**, *43*, 98.

(16) Chen, H.; Tagore, R.; Das, S.; Incarvito, C.; Faller, J. W.; Crabtree, R. H.; Brudvig, G. W. *Inorg. Chem.* **2005**, *44*, 7661.

(17) Chen, H.; Faller, J. W.; Crabtree, R. H.; Brudvig, G. W. *J. Am. Chem. Soc.* **2004**, *126*, 7345.

(18) Baffert, C.; Romain, S.; Richardot, A.; Lepretre, J.-C.; Lefebvre, B.; Deronzier, A.; Collomb, M.-N. *J. Am. Chem. Soc.* **2005**, *127*, 13694.

(19) Wolpher, H.; Huang, P.; Borgstroem, M.; Bergquist, J.; Styring, S.; Sun, L.; Akermark, B. *Catal. Today* **2004**, *98*, 529.

(20) Yagi, M.; Narita, K. *J. Am. Chem. Soc.* **2004**, *126*, 8084.

(21) Collomb, M. N.; Deronzier, A.; Richardot, A.; Pecaut, J. *New J. Chem.* **1999**, *23*, 351.

(22) Cooper, S. R.; Calvin, M. *J. Am. Chem. Soc.* **1977**, *99*, 6623.

(23) Manchanda, R.; Brudvig, G. W.; Degala, S.; Crabtree, R. H. *Inorg. Chem.* **1994**, *33*, 5157.

(24) Visser, H.; Anxolabe, E.; Lhe‘re-Mallart; Bergmann, U.; Glatzel, P.; Robblee, J. H.; Cramer, S. P.; Girerd, J.-J.; Sauer, K.; Klein, M. P.; Yachandra, V. K. *J. Am. Chem. Soc.* **2001**, *123*, 7031.

(25) In the earlier communication,[20] we considered that **1** is adsorbed on kaolin as the $Mn^{IV}-Mn^{IV}$ state on the basis of the UV−vis diffuse reflectance spectroscopic data. However, we reconsider that the species adsorbed on kaolin is the $Mn^{III}-Mn^{IV}$ state from the present Mn K-edge XANES data for the **1**/mica hybrid.

(26) Shimizu, K.; Maeshima, H.; Yoshida, H.; Satsuma, A.; Hattori, T. *Phys. Chem. Chem. Phys.* **2001**, *3*, 862.

(27) George, S. J.; Lowery, M. D.; Solomon, E. I.; Cramer, S. P. *J. Am. Chem. Soc.* **1993**, *115*, 2968.

(28) Farges, F.; Brown, G. E., Jr.; Rehr, J. J. *Phys. Rev. B* **1997**, *56*, 1809.

(29) Linkous, C. A.; O'Grady, W. E.; Sayers, D.; Yang, C. Y. *Inorg. Chem.* **1986**, *25*, 3761.

(30) Westre, T. E.; Kennepohl, P.; DeWitt, J. G.; Hedman, B.; Hodgson, K. O.; Solomon, E. I. *J. Am. Chem. Soc.* **1997**, *119*, 6297.

(31) Roe, A. L.; Schneider, D. J.; Mayer, R. J.; Pyrz, J. W.; Widom, J.; Que, L. *J. Am. Chem. Soc.* **1984**, *106*, 1676.

(32) Chen reported that a linear tetranuclear Mn^{IV} complex is slowly formed from $Mn^{IV}-Mn^{IV}$ in an acidic aqueous solution, which is shown by the absorption spectral change with the absorption decrease at 400−420 nm and the increase at 470 nm.[17] The formation of the linear tetranuclear Mn^{IV} complex was not observed up to 100 min under the conditions of 1.0 mM **1** and pH = 1.0 in the present work.

(33) Kaneko reported that O_2 is evolved when a Ce^{IV} oxidant is added to an aqueous suspension of **2**/kaolin.[9] However, the turnover numbers (0.38∼0.76) of **2** was less than unity, which is consistent with the present data. In the present work, the decomposition of **2** or **3** to form MnO_4^- ions was observed after the reaction for a **2** or **3** solution and **2** or **3**/clay.

(34) We confirmed that MnO_4^- cannot be adsorbed on mica and kaolin at all. Other cationic decomposed species might be adsorbed on clay, but they are not analyzed sufficiently.

(35) The plots of n_{MnO4-} versus n_{ads} should give an upward curvature as a MnO_4^- ion is formed by a bimolecular reaction of **1** for **1**/mica. However, these plots declined at high n_{ads}. This can be explained by side reactions with a consumption of the formed MnO_4^- ion at high n_{ads}. The consumption of the MnO_4^- ion formed was observed in a solution under the conditions of 0.1 mM **1** and 10 equiv Ce^{IV} after 30 min.